Angewandte Chemie International Edition

Angewandte International Edition Chemie

How to cite: *Angew. Chem. Int. Ed.* **2026**, e9951729
doi.org/10.1002/anie.9951729

RESEARCH ARTICLE

Lithium-Germanium Alloy Interfaces for Efficient Low-Pressure Ammonia Synthesis

Weijian Yang[1,2] | Pengju Li[2] | Kaining Duanmu[1] | Zijian Zhao[2] | Limei Tian[2] | Dan-Dan Zhai[2] | Benjamin D. Sherman[3] | Mark G. Humphrey[4] | Zhang-Jie Shi[2] | Chi Zhang[1] | Ke Hu[1,2]

[1]School of Chemical Science and Engineering, Tongji University, Shanghai, P. R. China | [2]Department of Chemistry and Shanghai Key Laboratory of Molecular Catalysis and Innovative Materials, Fudan University, Shanghai, P. R. China | [3]Department of Chemistry and Biochemistry, Louise Dilworth Davis College of Science and Engineering, Texas Christian University, Fort Worth, Texas, USA | [4]Research School of Chemistry, Australian National University, Canberra, Australia

Correspondence: Zhang-Jie Shi (zjshi@fudan.edu.cn) | Chi Zhang (chizhang@tongji.edu.cn) | Ke Hu (khu@tongji.edu.cn; khu@fudan.edu.cn)

Received: 25 December 2025 | **Revised:** 27 April 2026 | **Accepted:** 12 May 2026

Keywords: adsorption energy | electrochemical cycling | lithium alloy | lithium-mediated | nitrogen reduction reaction

ABSTRACT

The lithium-mediated nitrogen reduction reaction (Li-NRR) offers a sustainable pathway for ammonia synthesis, providing a viable alternative to the energy-intensive Haber-Bosch process. While most prior studies focused on solution-phase optimization, we introduce a transformative electrode engineering strategy via the rational design of triethylammonium germanate-modified copper (Cu/TEG) electrodes. Multi-technique characterization reveals the formation of the $Li_{15}Ge_4$ alloy during the Li-NRR. Electrochemical measurements combined with DFT calculations demonstrate that the $Li_{15}Ge_4$ alloy simultaneously facilitates lithium deposition and shifts the N_2 adsorption energy more exothermic. Most importantly, this interfacial engineering enables a Faradaic efficiency (FE) of up to 92.5% at an unprecedented N_2 pressure as low as 4 bar and with minimal overpotential relative to the onset of lithium deposition. This synergy minimizes energy losses, achieving the highest reported pseudo-energy efficiency value (17.6%) in a batch cell to the best of our knowledge. Overall, this work establishes dual-function interfacial engineering via lithium-germanium alloy formation as a breakthrough strategy, moving beyond conventional solution-phase optimization to provide a new approach for efficient electrochemical nitrogen fixation.

1 | Introduction

Ammonia is critical to global agriculture, sustaining the growing world population for over a century, with its annual production now exceeding 180 million tons [1–4]. However, industrial synthesis of ammonia via the Haber-Bosch process requires extremely high energy inputs and operates under harsh reaction conditions (350–450 °C, 10–20 MPa) [5], resulting in tremendous energy consumption and substantial carbon dioxide emissions [6], compelling urgent development of sustainable alternatives. In this regard, electrochemical ammonia synthesis under mild conditions has emerged as a promising pathway. The field has evolved rapidly, with high-efficiency protocols now established for various nitrogenous precursors, including N_2, NO, NO_2^-, and NO_3^- [7–10]. Recent progress has moved beyond catalyst discovery toward system-level engineering, such as chemometrics-boosted evaluation protocols [11], optimized flow-cell designs for enhanced transport [12], and advanced interface modulation [13]. Among these strategies, the lithium-mediated nitrogen reduction reaction (Li-NRR) is particularly noteworthy for its

Weijian Yang, Pengju Li, and Kaining Duanmu contributed equally to this work.

unique ability to spontaneously cleave the inert N≡N bond (941 kJ/mol) under ambient conditions to form Li_3N, with the latter subsequently undergoing protonation to yield NH_3 [14, 15]. Pioneered by Fichter et al. in 1930 and advanced through high-pressure optimization [16] and then isotopic validation [17], modern electrochemical Li-NRR achieves near-unity FE under high-pressure N_2 conditions [18, 19], positioning it as a transformative successor to conventional thermocatalysis.

Current research on the Li-NRR has largely been focused on optimizing solution parameters such as the electrolyte [18, 20–22], solvent [23–28], and proton donors [29–33]. In addition to this, several recent studies have focused on the electrode interface evolution and reaction mechanisms [34–36], which are essential for ensuring the fidelity of nitrogen fixation and guiding the rational design of Li-NRR systems. However, the fundamental constraints of the electrode interface leave plenty of scope for optimization. Conventional electrode substrates, such as foils, wires, or mesh made of metals such as copper, nickel, and iron [37, 38], do not facilitate lithium deposition. This inherent incompatibility forces the system to operate at high overpotentials, which leads to competing reactions, the formation of an excessively thick solid-electrolyte interphase (SEI) on the electrode surface, and significantly increased energy consumption [39]. Consequently, the overall Li-NRR efficiency decreases, resulting in low energy efficiency (EE). Further complicating matters, the inherently low solubility of N_2 in organic solvents typically necessitates high-pressure operations (> 15 bar) for efficient nitrogen fixation, presenting a major obstacle for green synthesis.

In contrast to solution-phase tuning, electrode surface engineering may represent another effective strategy [35, 39–43]. Lithium-containing alloy materials are frequently utilized to lower the lithium plating overpotential [44–48] (e.g., AgLi, with a ca. 85% FE) [40]. A central challenge for advancing Li-NRR is to lower the high N_2 pressure required to achieve a high FE. Given that electrode modification reliably enhances gas-molecule adsorption in electrocatalysis [49–51], and that Li-Ge alloys reshape the electron cloud density of Li in ways that could potentially strengthen N_2 adsorption [52–54], we turned to Group IVA elements (such as silicon, germanium, and selenium) to alloy with Li in pursuit of lower overpotential under milder N_2 pressure.

Herein, we introduce a novel electrode architecture for the electrochemical Li-NRR by integrating triethylammonium germanate (TEG) onto copper foil (Cu/TEG) to simultaneously facilitate lithium deposition and N_2 adsorption (Scheme 1). This strategy achieves a remarkable FE of 92.5% for NH_3 synthesis at a significantly reduced applied-potential (E_{app}) of −0.36 V vs $Li^{0/+}$ (all potentials are reported vs $Li^{0/+}$ unless otherwise noted) under a N_2 pressure as low as 4 bar. The reduced E_{app} dramatically decreases energy losses, enabling this approach to achieve the highest reported batch cell pseudo-EE value of 17.6%, to the best of our knowledge [55, 56]. Comprehensive characterization confirms the in situ formation of the $Li_{15}Ge_4$ alloy at the electrode interface. Electrochemical characterization, DFT calculations, and nitrogen fixation performance testing indicate that this alloy simultaneously facilitates lithium deposition and exothermically shifts the N_2 adsorption energy. The synergy between the efficient lithium plating and the enhanced nitrogen adsorption enables breakthrough performance under more mild conditions, opening up a new path for efficient and sustainable NRR systems.

2 | Results and Discussion

2.1 | Fabrication and Characterization of Cu/TEG Electrode

The TEG was synthesized from the reaction between triethylamine (TEA) and germanium dioxide [46], yielding $Et_3NH^+HGeO_3^-$ as shown in Equation 1:

$$GeO_2 + Et_3N + H_2O \rightarrow Et_3NH^+HGeO_3^- \quad (1)$$

The Cu/TEG electrode was fabricated via a scalable drop-casting method (Figure 1a). Post-synthesis scanning electron microscopy (SEM) revealed homogeneous TEG coverage with uniform morphology across the electrode surface (Figure 1b, S1). X-ray diffraction (XRD) analysis revealed the presence of crystalline GeO_2, while no signal for the C—N species of the TEG was detected (Figure S2). The existence of NH and $HGeO_3$ species was confirmed using Fourier transform infrared spectroscopy (FTIR, Figure S3). In contrast to TEA or GeO_2, TEG displays prominent peaks corresponding to NH and $HGeO_3$ in the FTIR spectrum, providing solid evidence for the generation of TEG rather than a physical mixture of TEA and GeO_2. To elucidate the detailed chemical composition of the TEG layer, x-ray photoelectron spectroscopy (XPS) analysis was carried out. The surface XPS profile indicated the presence of C, Ge, O, and N elements in the TEG layer, with the N 1s and Ge 3d peaks at 401.2 and 33.1 eV corresponding to C—N and Ge—O groups, respectively, in agreement with the featured components of $Et_3NH^+HGeO_3^-$ (Figure 1c,d and Figure S4).

Following the successful fabrication of the Cu/TEG electrode via drop-casting, its electrochemical behavior was systematically evaluated to assess its Li-NRR applicability. Linear sweep voltammetry (LSV) curves showed a distinct positive shift in the onset potential for Li^+ reduction on Cu/TEG relative to bare Cu (Figure 2a). Crucially, this modified electrode achieves identical current density at a 0.7 V lower E_{app}, which is attributed to the in situ formation of a conductive Li_xGe alloy surface coating that lowers the nucleation barrier, as reported by Sun et al., [46]. Complementary cyclic voltammetry (CV) curves indicated that the modified electrode displayed minimal voltage hysteresis during Li plating/stripping (Figure 2a, insert), indicative of reduced overpotential compared to the copper foil electrode, and more efficient Li cycling owing to the formation of the Li_xGe alloy [40].

Electrochemical impedance spectroscopy (EIS) measurements were employed to further assess the charge transfer kinetics for the reduction of Li^+ in solution [57]. EIS spectra fitted using a Randle's equivalent circuit revealed that the Cu/TEG electrode exhibited reduced charge transfer resistance (R_{ct} of 134 Ω, Figure 2b) compared to the Cu electrode (189 Ω). This shows that the higher currents observed at comparable applied bias for Li^+ reduction in the LSV/CV experiments arise from more rapid interfacial electron transfer. This synergistic enhancement of the lowered overpotential, improved reversibility, and more

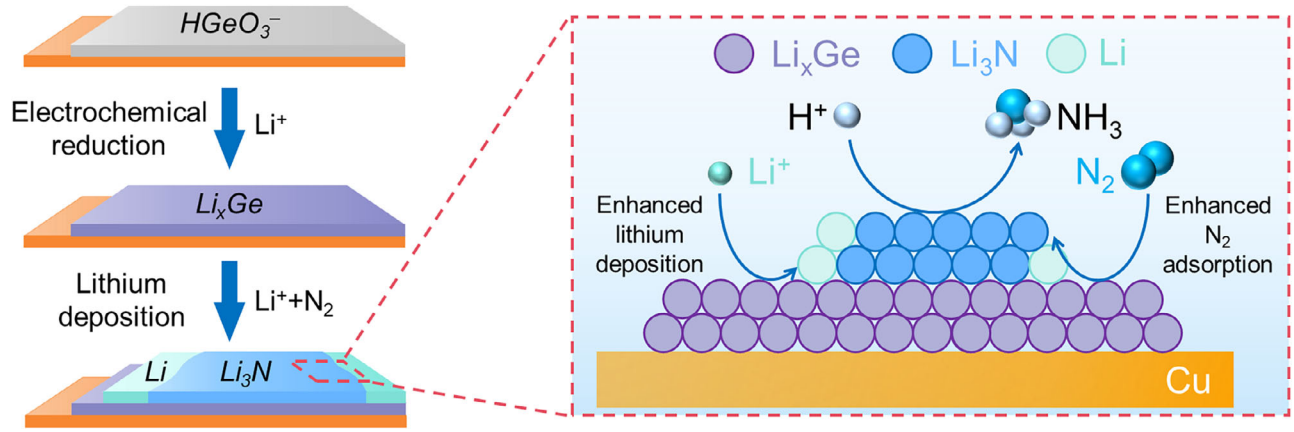

SCHEME 1 | Schematic process for the electrochemical Li-NRR operating at a Cu/TEG electrode.

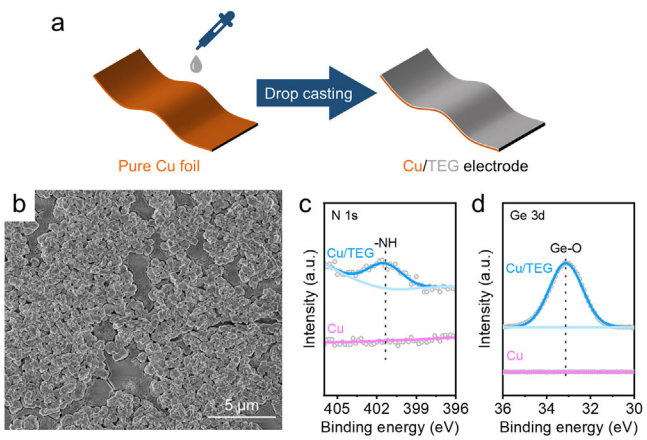

FIGURE 1 | (a) Schematic illustration of the drop-casting method for the preparation of Cu/TEG. (b) SEM images of Cu/TEG. High-resolution XPS spectra of the N 1s (c) and Ge 3d (d) for bare Cu foil and Cu/TEG.

rapid interfacial charge transfer collectively establishes Cu/TEG as an advanced Li-NRR electrode platform.

2.2 | Electrochemical Li-NRR Performance

Following validation of the enhanced electrochemical Li^+ reduction performance of the Cu/TEG electrode, systematic investigations of electrochemical Li-NRR in a batch cell configuration were performed. Initial optimization studies screened critical solution parameters including various lithium electrolytes and proton donors (Figure S5 and S6). After comprehensive evaluation, THF containing 1.5 M $LiClO_4$ and 150 mM *n*-butanol was identified as the optimal electrolyte composition. Additionally, a detailed screening of the electrode thickness in drop-coating was performed (Figure S7b). Assessment of the Li-NRR performance was then carried out with different E_{app} (Figure S7a), achieving an outstanding FE of 27.0% at just 60 mV of overpotential relative to lithium reduction (E_{app} = -0.06 V vs $Li^{0/+}$) under 1 atm N_2.

Our investigations revealed outstanding FE at 0 V and even at an applied bias positive of $Li^{0/+}$, demonstrating an excellent nitrogen-fixation capability. This is in stark contrast to the unmodified copper foil electrode, which showed no production of ammonia at −0.06 V versus $Li^{0/+}$ (0% FE), and with only a slight activity (2.4% FE) at a significantly more negative potential of −0.76 V under identical experimental conditions (Figure 2c). The substantially reduced E_{app} and the enhanced FE observed in the Li-NRR are attributable to the formation of Li_xGe species at the electrode interface. This will be expounded further in the mechanistic investigations that follow.

To further elucidate the formation of possible byproducts, gas chromatography (GC) was employed to analyze the headspace gas composition following performance of the Li-NRR. The results indicated minor production of H_2 as a byproduct with a FE of 19.7% (Figure S9). It was postulated that the observed loss in FE might stem from the reaction of metallic lithium with N_2 or the protonation of Li_3N. Due to the limited solubility of N_2 in THF, the sluggish reaction kinetics between the generated metallic lithium and N_2 likely results in the formation of a thick layer of deposited metallic lithium, leading to reduced reaction activity.

Subsequent work found that elevated pressure can significantly increase the solubility of N_2 in THF and to some extent, suppress electrochemical H_2 production [58, 59]. Consequently, Li-NRR experiments were conducted at varied N_2 pressures (Figure 3a), demonstrating a rapid increase in FE with increasing pressure until a plateau was reached at approximately 4 bar of N_2, beyond which the FE remained relatively stable. This trend aligns with prior high-pressure Li-NRR observations, but manifests itself at substantially lower pressures in our system. Optimization of the applied potential under 4 bar N_2 (Figure S10a) identified an optimal operating potential of −0.36 V. This cathodically shifted potential is mechanistically linked to an increase in kinetics of the reaction between reduced metallic lithium and dissolved N_2, although a detailed investigation of this phenomenon extends beyond the scope of the present study.

Prolonged Li-NRR experiments under the aforementioned conditions using a reduced electrode area (0.08 cm^2) exhibited a sustained FE around 92.5%, a noteworthy ammonia production rate of 138 $nmol \cdot s^{-1} \cdot cm^{-2}$, and a consistent current density of 40–50 $mA \cdot cm^{-2}$, without any discernible decrease after 12 h (Figure 3c). Additionally, H_2 byproduct was quantified with a FE of approximately 7.0% ± 0.2% (Figure S11), bringing the total

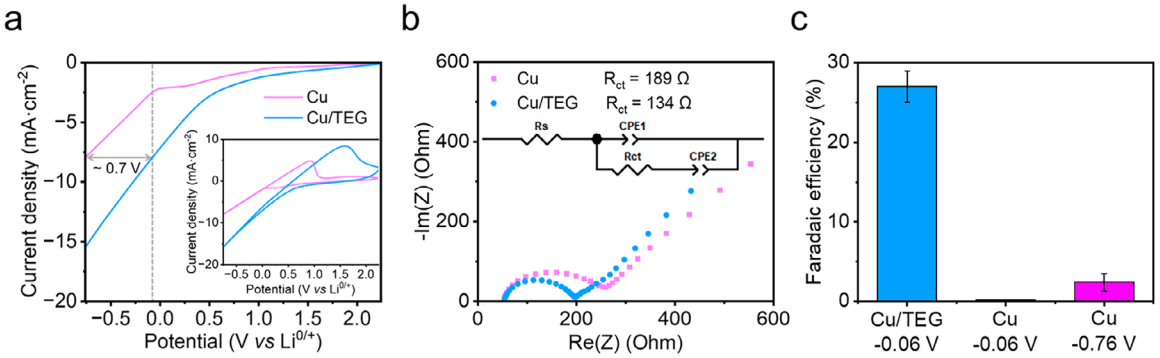

FIGURE 2 | (a) LSV curves of Cu/TEG and bare Cu foil. Insert: CV curves of Cu/TEG and bare Cu foil. (b) EIS spectra of Cu/TEG and Cu foil measured at 0 V vs $Li^{0/+}$. (c) Li-NRR performance of Cu/TEG and bare Cu under 1 bar of N_2. Error bars represent the standard deviation calculated from three independent parallel experiments.

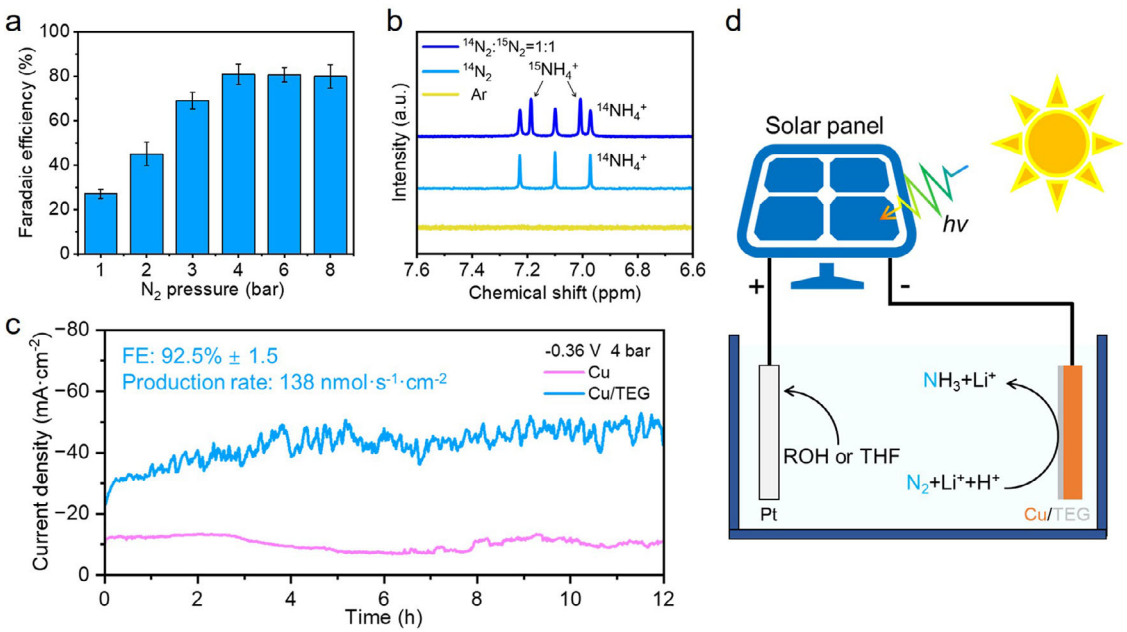

FIGURE 3 | (a) FE of Li-NRR using a Cu/TEG electrode as a function of N_2 pressure with $E_{app} = -0.36$ V (for 1 bar, $E_{app} = -0.06$ V); Error bars represent the standard deviation calculated from three independent parallel experiments. (b) ^{1}H NMR spectra of ammonia by using Ar, $^{14}N_2$, or $^{14}N_2$:$^{15}N_2 = 1{:}1$ as feed gas. (c) Long-term Li-NRR performance with an electrode active area of 0.08 cm^2. (d) Schematic illustration of the self-powered Li-NRR system using solar light.

FE to nearly 100%. This decrease in H_2 FE compared to the 1 atm N_2 condition (19.7%) confirms that elevated N_2 pressure can effectively suppress the competitive hydrogen evolution reaction, consistent with literature reports [58, 59]. When an excess of proton donor was introduced the electrode exhibited a stable operation for over 90 h without significant current decrease, although a sustained operation was hindered by the continuous depletion of the proton donor (Figure S12). This performance is in stark contrast to that of bare copper foil electrodes, which yielded only 16.0% FE at approximately 10 $mA{\cdot}cm^{-2}$ under identical conditions (Figure S13a). Control experiments coupled with $^{15}N_2$ isotope labeling conclusively established molecular nitrogen as the exclusive ammonia precursor, verified via ^{1}H nuclear magnetic resonance (NMR) analysis (Figure 3b). Under an argon atmosphere, no characteristic ammonia signals emerged in the range 7.4–6.9 ppm, while under a pure $^{14}N_2$ atmosphere, a characteristic triplet peak corresponding to $^{14}NH_4^+$ was evident and under an atmosphere of 1:1 $^{14}N_2$:$^{15}N_2$, the overlapping triplet peak of $^{14}NH_4^+$ and doublet peak of $^{15}NH_4^+$ maintained an integral ratio of 1:1, confirming the nitrogen origin as N_2 rather than other possible sources.

Cross-validation of the ammonia quantification via indophenol blue colorimetric and ^{1}H NMR analysis revealed excellent agreement within experimental error (Figures S13b, S14 and S15). Furthermore, to eliminate the possibility of false-positive results, systematic pollution-excluding detections were conducted [27], including for NH_3 pollution (Figure S16), nitrogen oxides (NO_x) contaminants, and byproduct N_2H_4 content (Figure S17). According to the comprehensive results, no detectable NH_3 pollution or NO_x contaminants were observed across these components prior to the reaction. Although trace amounts of N_2H_4 (< 0.6 ppm) were

detected after the 12 h Li-NRR, the corresponding FE was negligible (< 0.1%). These rigorous validation tests confirm that the measured NH_3 is intrinsically derived from the electrochemical Li-NRR process, ensuring the reliability and authenticity of the high-efficiency nitrogen fixation achieved by this system.

Additionally, Li-NRR experiments were conducted at various reaction time intervals (3, 6, 9, and 12 h) involving different total charge accumulations. Ammonia quantification across these conditions consistently yielded FEs of approximately 90%, with the 12 h test reaching an FE of 90.9% ± 4.2%, demonstrating excellent repeatability (Figure S18). Combined with numerous repeated trials, these results allow us to confidently conclude that the high FE achieved with the modified Cu/TEG electrode is not an incidental occurrence, but is consistently reproduced across multiple independent electrode batches and varying reaction durations.

Subsequently, to minimize the reliance on electrical energy as a secondary energy source, two strategies were tested to integrate light energy as a renewable energy source into the electrocatalytic system, thereby reducing the external electrical energy input. The first approach entails the integration of photovoltaic cells coupled with the electrocatalytic system. A self-powered system was established that harnesses photogenerated carriers from polycrystalline silicon solar panels, directing them to Cu/TEG electrodes for Li-NRR (Figure 3d). This configuration enables direct solar-driven Li-NRR without the need for external electrical energy, achieving an ammonia production rate of up to 79.9 $nmol \cdot s^{-1} \cdot cm^{-2}$. The second strategy involves substituting the Pt counter electrode with a Fe_2O_3 photoanode, leveraging the photogenerated holes from the photoanode to facilitate the oxidation reaction at the counter electrode. This modification significantly reduces the required cell voltage, yielding an intrinsic solar-to-chemical (ISTC) conversion efficiency as high as 2.43% (Figure S19). The implementation of these strategies aligns with the principles of green chemistry, enabling a synergistic photochemical-coupled-to-electrochemical approach to nitrogen fixation.

2.3 | Mechanistic Investigations

To explore the dynamic evolution of the electrode interface during the Li-NRR, and thereby uncover the origin of the enhanced performance, systematic electrochemical and interfacial characterizations were conducted. CV measurements were performed at a reduced scan rate of 1 $mV \cdot s^{-1}$ to obtain detailed insight, as shown in Figure 4a for the Cu/TEG electrode. In the initial cathodic scan, a broad shoulder was observed in the range 0.49 to 0.37 V, which corresponds to the irreversible formation of a solid electrolyte interface (SEI) [60] and diminishes in subsequent cycles. Another cathodic peak at approximately 0.18 V is attributed to the reversible alloying reaction of Li_xGe, while a peak at 0.26 V is indicative of the reversible delithiation of the Li_xGe alloy to Ge during the anodic scans [61, 62]. The observed alloying potential aligns with literature reports for $Li_{15}Ge_4$ formation, and we assign this phase based on two key factors: (i) The characteristic reduction potential matches the reported values for $Li_{15}Ge_4$ [61, 63]; (ii) Thermodynamic considerations suggest that $Li_{15}Ge_4$ is the predominant phase for cathodic polarization below the lithium plating potential (-0.36 V), as it exhibits the most negative formation potential for lithium-germanium alloys and it becomes energetically favored under strongly reducing conditions [64–66]. An additional anodic peak at 0.7 V is associated with the re-oxidation of surface Ge to GeO_2 [64]. The interfacial alloying reactions are shown in Equations 2–3: [67].

$$HGeO_3^- + 4Li^+ + 4e^- \rightarrow Ge + 2Li_2O + OH^- \quad (2)$$

$$Ge + xLi^+ + xe^- \leftrightarrow Li_xGe \quad (3)$$

The slight decrease in peak intensity in successive scans suggests the occurrence of irreversible processes during the initial cycle. For the pure Cu foil, no alloying reaction occurred (Figure S20).

To track the phase evolution and confirm the formation of the proposed alloy interface, we performed time-dependent ex situ XRD characterization at various reaction intervals (Figure 4b). The initial TEG diffraction peaks rapidly diminish within the first 20 s of electrolysis, followed by the emergence of distinct $Li_{15}Ge_4$ signals by 100 s. Crucially, the $Li_{15}Ge_4$ phase remains highly stable and shows no signs of degradation or phase transformation throughout the subsequent 7200 s of the Li-NRR process [46]. This observation confirms that the $Li_{15}Ge_4$ alloy is the genuine and stable catalytic interface during operation, which is further corroborated by in situ x-ray absorption near edge structure (XANES) analysis. Owing to the strong substrate interference from the copper foil that hinders high-quality in situ XRD measurements, in situ Ge K-edge XANES was performed to monitor the phase identity under actual working conditions (Figure S21). The XANES spectra exhibit a shift in the absorption edge toward lower energy and a decrease in white line intensity, consistent with the electronic signatures of $Li_{15}Ge_4$ alloys. [68, 69] These results provide direct in situ evidence for the generation and stable existence of the $Li_{15}Ge_4$ alloy on the electrode surface.

Consistent with the XRD results, time-of-flight secondary ion mass spectrometry (TOF-SIMS) was employed to further validate the interfacial composition upon electrochemical reduction (Figure 4c and Figure S22). Under N_2, distinct peaks corresponding to Li^- and Li_3N^- were observed in the negative TOF-SIMS spectrum, indicating the formation of Li_3N [46]. The presence of metallic lithium cannot be definitively confirmed, as the Li^- signal may arise from any lithium-containing compounds [70, 71]. Moreover, various CH and CN species were also detected, possibly originating from the SEI layer or the TEG. In the positive ion spectrum, a higher intensity of the Li^+ peak and a prominent $LiGe^+$ peak were seen, consistent with Li alloying with Ge. Under an argon atmosphere, peaks of $Li^{-/+}$ and $LiGe^+$ were present, while the Li_3N^- peak was absent, indicating that the generation of Li_3N necessitates N_2 involvement and that the $Li_{15}Ge_4$ alloy either exhibits limited reactivity with N_2 or has a slow reaction rate.

Time-resolved ex situ XPS was employed to investigate the evolution of interfacial species on the electrode at different reaction intervals under actual working conditions (Figure 4d–f). In the early stages of the reaction (0-100 s), the Ge 3d spectra show the transition from Ge^{4+} through a Ge^0 intermediate to the final $Li_{15}Ge_4$ alloy [72–75]. Interestingly, the N 1s and Li

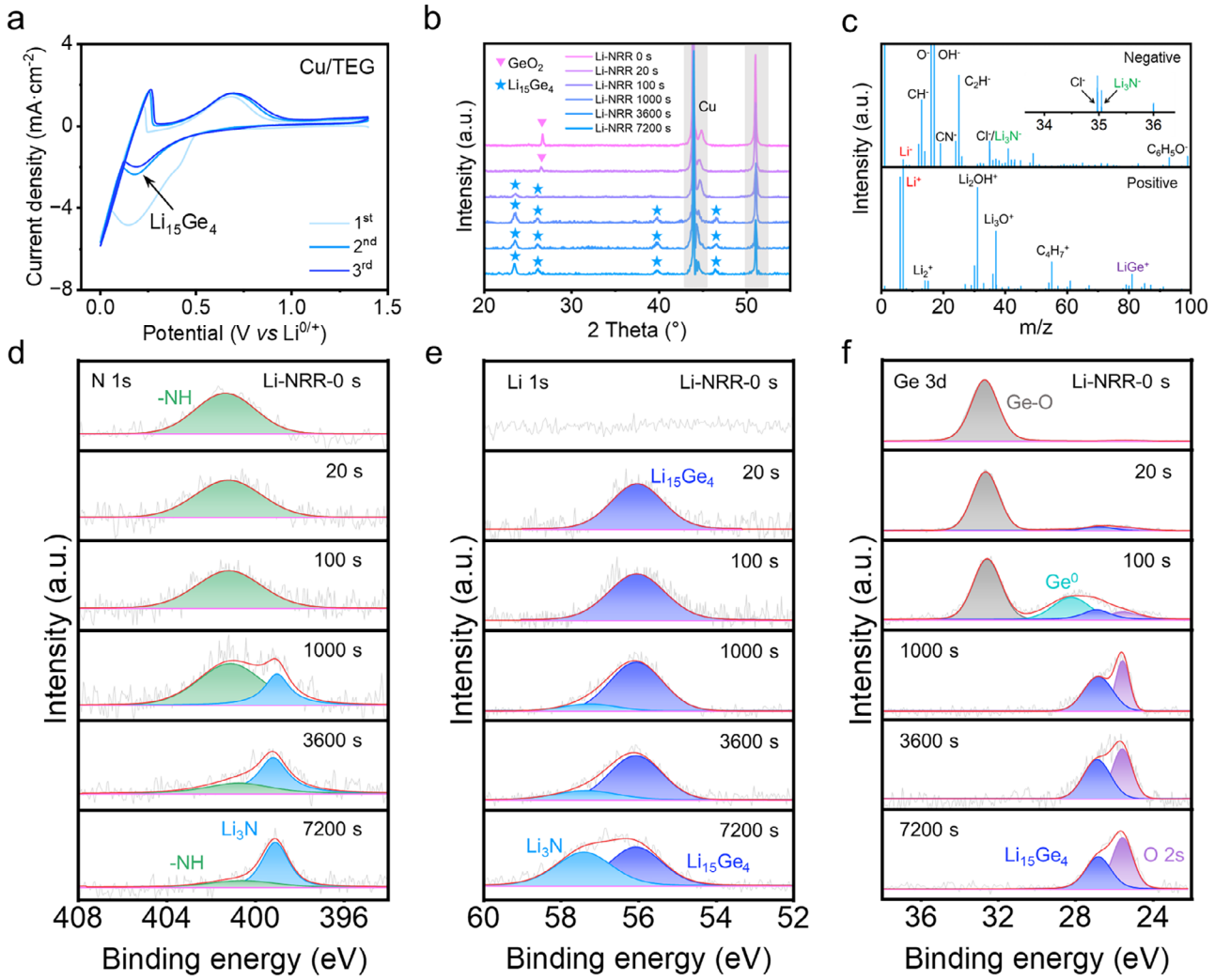

FIGURE 4 | (a) Repeat CV scans of a Cu/TEG electrode at a scan rate of 1 mV/s. (b) Time-dependent ex situ XRD patterns of the Cu/TEG electrode at various reaction intervals (0, 20, 100, 1000, 3600, and 7200 s) during the Li-NRR process. (c) Negative and positive TOF-SIMS spectra of Li_3N^-, $LiGe^+$, $Li^{+/-}$, and secondary ion fragments obtained on Cu/TEG after electrochemical Li-NRR under N_2 atmosphere. (d–f) Time-dependent ex situ high-resolution XPS spectra for N 1s, Li 1s, and Ge 3d of the Cu/TEG electrode at various reaction intervals (0, 20, 100, 1000, 3600, and 7200 s) during the Li-NRR process. The intensities are normalized for better visualization of the chemical state evolution.

1s spectra indicate that Li_3N formation is negligible during the initial alloying period (0-100 s) [75], suggesting that Li^+ reduction is initially consumed for $Li_{15}Ge_4$ alloy interface construction. Significant Li_3N signals only appear after the complete formation of the $Li_{15}Ge_4$ interface, confirming that the alloy phase acts as the prerequisite platform for nitrogen fixation.

In the triethylammonium germanate electrode material, the germanate anion serves as the pivotal component by forming a $Li_{15}Ge_4$ alloy, which facilitates uniform and dense lithium deposition. Concurrently, the incorporation of triethylammonium cations aids in transforming the initially turbid GeO_2 suspension into a stable colloidal dispersion of TEG, thereby promoting the formation of a more homogeneous and robust electrode structure. As a result, Cu/TEG exhibits a significantly enhanced electrochemical performance compared to a Cu/GeO_2 electrode. However, triethylamine itself does not directly contribute to the nitrogen fixation performance; the GeO_2—capable of alloying with Li^+ to form $Li_{15}Ge_4$—remains the key active species (Figure S10b).

Multi-technique characterization unambiguously identified two critical interfacial species after the Li-NRR: The $Li_{15}Ge_4$ alloy and Li_3N. While Li_3N serves as the pivotal nitrogen fixation intermediate, the precise role of the $Li_{15}Ge_4$ alloy remains elusive. Prior research indicated that, the formation of the $Li_{15}Ge_4$ alloy enhances the reduction of Li^+ to metallic lithium by offering enhanced adsorption capacity, increased nucleation sites, and diminished energy barriers due to the strong interaction between $Li_{15}Ge_4$ and Li^+ [46, 47]. Electrochemical characterizations performed herein, including LSV, CV, and EIS, demonstrates that the modified electrode exhibits enhanced lithium deposition kinetics (Figure 2a–c). Consequently, we attribute the improved performance of the Cu/TEG electrode in the Li-NRR to the presence of the $Li_{15}Ge_4$ alloy.

Although the $Li_{15}Ge_4$ alloy facilitates Li^+ reduction, the ability to achieve over 90% FE at N_2 pressures as low as 4 bar remains an intriguing and unexplained observation, especially since prior reports required significantly higher pressures. This unexpected

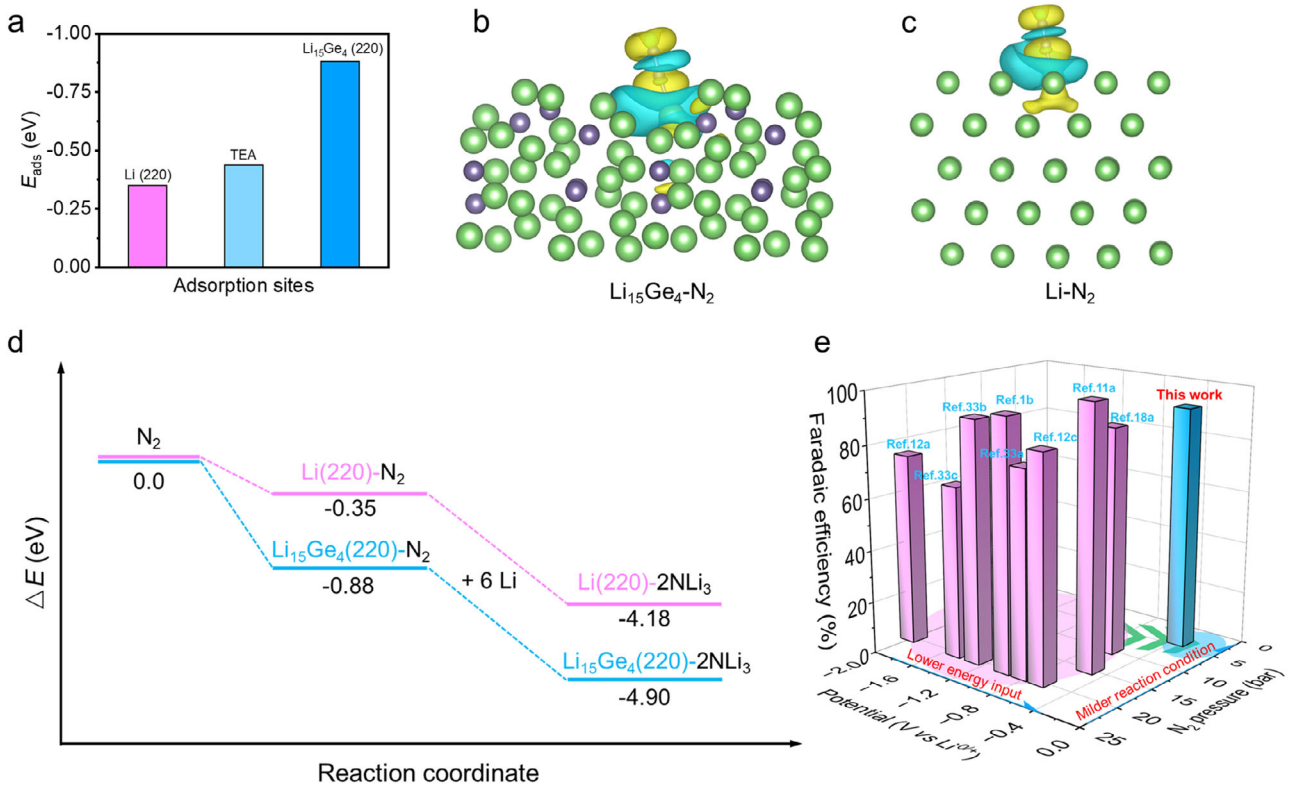

FIGURE 5 | (a) Adsorption energy (E_{ads}) of N_2 molecule adsorbed on Li(220), triethylamine (TEA), and $Li_{15}Ge_4$(220). (b, c) Optimized structures and charge density difference plots of N_2 molecular adsorption on $Li_{15}Ge_4$ and metallic Li, respectively. (d) Calculated electronic energy steps for N_2 adsorption and Li_3N formation on $Li_{15}Ge_4$(220) and metallic Li(220) surfaces. (e) A comparison of the maximum Faradaic efficiencies reported for different strategies using batch cells under different N_2 pressure and E_{app}.[2, 18, 20, 22, 40, 76–78].

finding suggests that, beyond elevated pressure-induced increase in N_2 solubility, an additional mechanism may be at play that promotes interfacial N_2 accessibility at the electrode surface in our system. This is supported by the fact that, the Cu/TEG electrode achieves FE saturation at merely 4 bar, whereas a bare Cu electrode requires a much higher pressure of approximately 12 bar to reach its performance plateau (Figure S23). We hypothesized that the modified electrode surface possesses an enhanced capability for N_2 adsorption, which facilitates more effective capture of dissolved nitrogen at the interface.

To examine this hypothesis, DFT calculations were performed to compare N_2 adsorption on the $Li_{15}Ge_4$ alloy interfaces and metallic Li. Among the calculated $Li_{15}Ge_4$ surfaces, the (220) facet showed the strongest N_2 adsorption, consistent with the dominant x-ray diffraction pattern observed experimentally (Figure 4b); detailed surface models and adsorption energies are provided in the Supporting Information (Figure S24, S25, and Table S2). Using this representative surface, Figure 5a shows that N_2 adsorption on $Li_{15}Ge_4$ (220) is markedly stronger than that on metallic Li (220) and triethylamine, indicating that the alloy interface can serve as an effective N_2-enrichment site. Charge density difference (CDD) and Bader charge analyses reveal substantial electron redistribution upon N_2 adsorption (Figures 5b, c and S27 and 28), supporting a stronger interaction between N_2 and the alloy surface than that on metallic Li. This interaction can be rationalized by the electronic modulation of surface Li atoms by Ge, which increases their electropositivity and thereby enhances their affinity toward N_2. Importantly, the calculated electronic energy ($\triangle E$) profile for Li_3N formation shows that the $Li_{15}Ge_4$ interface provides a more thermodynamically favorable pathway than metallic Li (Figure 5d). Taken together, these results suggest that the in situ-formed $Li_{15}Ge_4$ alloy not only promotes Li deposition, as shown by the electrochemical characterizations, but also enriches dissolved N_2 at the electrode interface. The locally enriched N_2 can then react more efficiently with metallic Li generated in situ, facilitating Li_3N formation and, thereby contributing to the high FE observed at N_2 pressures as low as 4 bar.

Figure 5e compares the performance of our system with leading contemporary Li-NRR systems that typically rely on solution-phase strategies and require significantly higher overpotentials and N_2 pressures to achieve comparable FE. This comparison highlights our system operation under significantly milder conditions, in particular the lowest reported E_{app} of −0.36 V, while using 3–5 times lower N_2 pressure (4 bar) than existing high-performance systems. This breakthrough performance is attained through targeted electrode surface modification, for which electrochemical characterization and DFT calculations demonstrate that the in situ-generated $Li_{15}Ge_4$ concurrently enhances lithium deposition kinetics and facilitates N_2 adsorption. Crucially, EE serves as an essential metric for evaluating overall energy conversion in the production process. In a batch cell, pseudo-EE was used as an academic indicator that estimates the EE based on the ratio of the free-energy change of

the ammonia formation reaction to the total electrical energy input, without considering industrial operational factors such as hydrogen recycling (see Supporting Information for calculation details) [14, 25, 56, 79, 80]. Our electrode engineering strategy substantially reduces both the overpotential and N_2 pressure, enabling a pseudo-EE of 17.6%, which is the highest reported value in a batch cell to the best of our knowledge (Table S1). This represents a six-fold enhancement over unmodified copper electrodes and demonstrates that our modification approach minimizes energy losses in lithium-mediated nitrogen fixation, representing a critical step toward environmentally benign green ammonia synthesis. Notably, while most published reports of Li-NRR are conducted at significantly higher N_2 pressures (typically 15–20 bar) [2, 18, 20, 25, 40, 56, 76–78, 81, 82], the approach described here operates under much milder conditions (4 bar). To further substantiate this energetic advantage, we benchmarked our system against several state-of-the-art systems by calculating their pseudo-EE at comparable low pressures (ca. 4–5 bar) based on their reported pressure-dependent performance curves [18, 20, 81, 82]. Under these equivalent low-pressure conditions, our system achieves a pseudo-EE that is 2–4 times higher than other comparative studies, further confirming the energetic advantage of this system.

3 | Conclusion

In summary, this work demonstrates that forming a $Li_{15}Ge_4$ alloy at the interface fundamentally alters the reaction pathway for lithium-mediated nitrogen reduction. Using the triethylammonium germanate-modified copper (Cu/TEG) electrode, ammonia production was achieved at 92.5% FE, with a significantly reduced applied potential of −0.36 V vs $Li^{0/+}$ and at N_2 pressures as low as 4 bar. Such conditions were previously considered unsuitable for efficient NH_3 synthesis, establishing that electrode engineering can overcome intrinsic limitations of Li-NRR systems. The dual functionality of the alloy interface, simultaneously accelerating Li^+ deposition while enhancing N_2 adsorption, enabled the highest reported pseudo-energy efficiency (17.6%) in a batch cell (to the best of our knowledge), and reveals a previously unexplored reaction mechanism for nitrogen fixation. Finally, we designed two approaches for introducing light energy into the electrochemical system, thereby enabling photo-driven electrochemical nitrogen fixation, which significantly reduces electrical energy consumption and improves overall energy utilization efficiency. These findings motivate targeted phase design strategies to unlock energetically efficient routes for sustainable ammonia electrosynthesis.

Author Contributions

Weijian Yang: Writing – review and editing, writing – original draft, methodology, data curation, investigation, formal analysis, visualization, and validation. **Pengju Li:** Methodology, data curation, investigation, validation, formal analysis, and writing – review and editing. **Kaining Duanmu:** Visualization, writing – review and editing, software, formal analysis, data curation, investigation, and methodology. **Zijian Zhao:** Formal analysis, investigation, writing – review and editing, and funding acquisition. **Limei Tian:** Investigation, formal analysis, and writing – review and editing. **Dan–Dan Zhai:** Methodology, resources, writing – review and editing. **Benjamin D. Sherman:** Writing – review and editing. **Mark G. Humphrey:** Writing – review and editing. **Zhang–Jie Shi:** Methodology, supervision, project administration, resources, and writing – review and editing. **Chi Zhang:** Supervision, project administration, resources, writing – review and editing, and funding acquisition. **Ke Hu:** Conceptualization, methodology, formal analysis, supervision, funding acquisition, visualization, project administration, resources, writing – original draft, writing – review and editing, and validation.

Acknowledgments

This work is sponsored by the National Key R&D Program of China (2023YFE0124100), the National Natural Science Foundation of China (22173022, 22588201, 22201044), the Fundamental Research Funds for the Central Universities, and the China Postdoctoral Science Foundation (2025T180305, 2024M760508, GZB20240159). The authors sincerely thank Prof. Degao Wang from the Ningbo Institute of Materials Technology and Engineering (NIMTE), Chinese Academy of Sciences, and Prof. Yonggang Wang and Prof. Liming Zhang from the Department of Chemistry, Fudan University, for their valuable assistance with material characterization. This work was also supported by the user experiment assist system of the Shanghai Synchrotron Radiation Facility (SSRF). The authors thank beamline BL14W1 at SSRF for providing the beam time.

Conflicts of Interest

The authors declare no conflicts of interest.

Data Availability Statement

The data that support the findings of this study are available from the corresponding author upon reasonable request.

References

1. N. H. Deissler, J. B. V. Mygind, K. Li, et al., "Operando Investigations of the Solid Electrolyte Interphase in the Lithium Mediated Nitrogen Reduction Reaction," *Energy & Environmental Science* 17 (2024): 3482–3492, https://doi.org/10.1039/D3EE04235A.

2. S. Li, Y. Zhou, K. Li, et al., "Electrosynthesis of Ammonia With High Selectivity and High Rates via Engineering of the Solid-Electrolyte Interphase," *Joule* 6 (2022): 2083–2101, https://doi.org/10.1016/j.joule.2022.07.009.

3. J. Lim, C. A. Fernández, S. W. Lee, and M. C. Hatzell, "Ammonia and Nitric Acid Demands for Fertilizer Use in 2050," *ACS Energy Letters* 6 (2021): 3676–3685, https://doi.org/10.1021/acsenergylett.1c01614.

4. M. I. Ahmed, A. Assafiri, D. B. Hibbert, and C. Zhao, "Li-Mediated Electrochemical Nitrogen Fixation: Key Advances and Future Perspectives," *Small* 19 (2023): 2305616, https://doi.org/10.1002/smll.202305616.

5. X. Fu, J. Zhang, and Y. Kang, "Recent Advances and Challenges of Electrochemical Ammonia Synthesis," *Chem Catalysis* 2 (2022): 2590–2613, https://doi.org/10.1016/j.checat.2022.09.001.

6. Y. Chen, H. Liu, N. Ha, S. Licht, S. Gu, and W. Li, "Revealing Nitrogen-Containing Species in Commercial Catalysts Used for Ammonia Electrosynthesis," *Nature Catalysis* 3 (2020): 1055–1061, https://doi.org/10.1038/s41929-020-00527-4.

7. L. Huang, P. Zhang, X. Ge, et al., "Efficient Neutral Nitrate-to-Ammonia Electrosynthesis Using Synergistic Ru-Based Nanoalloys on Nitrogen-Doped Carbon," *Nano-Micro Letters* 18 (2025): 66, https://doi.org/10.1007/s40820-025-01896-w.

8. S. Chen, Y. Wei, Z. Zhang, et al., "Synergistic Promotion of Nitrate-to-Ammonia Electrosynthesis by Cyclodextrin-Modified Cu Nanoparticles," *Journal of Energy Chemistry* 115 (2026): 824–831, https://doi.org/10.1016/j.jechem.2025.12.017.

9. Z. Lu, J. Zhang, Y. Wang, Y. Yu, and L. Kong, "Recent Advances in Metal Single-Atom Catalysts for Ammonia Electrosynthesis," *Materials Horizons* 12 (2025): 3286–3300, https://doi.org/10.1039/D5MH00042D.

10. M. Biswas, S. J. Phukan, S. Goswami, et al., "Techno-Economic Insights Into Ammonia as a Hydrogen Vector: Synthesis, Cracking, Storage, and Supply Chain Solutions," *Green Chemistry* 28 (2026): 3963–4005, https://doi.org/10.1039/D5GC04925C.

11. N. Pirrone, S. Garcia-Ballesteros, J. Amici, M. Castellino, S. Hernández, and F. Bella, "Chemometrics-Boosted Protocols for Effortless Evaluation of Factors Affecting the Electrochemical Nitrate Reduction to Ammonia," *Journal of Energy Chemistry* 107 (2025): 599–611, https://doi.org/10.1016/j.jechem.2025.03.072.

12. N. Pirrone, S. Garcia-Ballesteros, S. Hernández, and F. Bella, "Membrane/Electrolyte Interplay on Ammonia Motion Inside a Flow-Cell for Electrochemical Nitrogen and Nitrate Reduction," *Electrochimica Acta* 493 (2024): 144415, https://doi.org/10.1016/j.electacta.2024.144415.

13. Y. Wang, S. Wang, Y. Fu, et al., "Ammonia Electrosynthesis From Nitrate Using a Stable Amorphous/Crystalline Dual-phase Cu Catalyst," *Nature Communications* 16 (2025): 897, https://doi.org/10.1038/s41467-025-55889-9.

14. S. Li, X. Fu, J. K. Nørskov, and I. Chorkendorff, "Towards Sustainable Metal-Mediated Ammonia Electrosynthesis," *Nature Energy* 9 (2024): 1344–1349, https://doi.org/10.1038/s41560-024-01622-7.

15. N. Lazouski and K. Manthiram, "Ambient Lithium-Mediated Ammonia Synthesis," *Trends in Chemistry* 1 (2019): 141–142, https://doi.org/10.1016/j.trechm.2019.02.008.

16. M. Jiang, X. Chen, F. Chen, et al., "Effective N_2 Activation Strategies for Electrochemical Ammonia Synthesis," *Chemistry* 11 (2025): 102441, https://doi.org/10.1016/j.chempr.2025.102441.

17. S. Z. Andersen, V. Čolić, S. Yang, et al., "A Rigorous Electrochemical Ammonia Synthesis Protocol With Quantitative Isotope Measurements," *Nature* 570 (2019): 504–508, https://doi.org/10.1038/s41586-019-1260-x.

18. H.-L. Du, M. Chatti, R. Y. Hodgetts, et al., "Electroreduction of Nitrogen With Almost 100% Current-to-Ammonia Efficiency," *Nature* 609 (2022): 722–727, https://doi.org/10.1038/s41586-022-05108-y.

19. H. Zhang, Z. Lu, and Z. Wen, "Advancing Lithium-Mediated Ammonia Synthesis," *Nature Reviews Chemistry* 9 (2025): 285–286, https://doi.org/10.1038/s41570-025-00709-3.

20. H. Yun, C. Lim, M. Kwon, et al., "Localized High-Concentration Electrolyte in Li-Mediated Nitrogen Reduction for Ammonia Synthesis," *Advanced Materials* 36 (2024): 2408280, https://doi.org/10.1002/adma.202408280.

21. X. Fu, S. Li, N. H. Deissler, J. B. V. Mygind, J. Kibsgaard, and I. Chorkendorff, "Effect of Lithium Salt on Lithium-Mediated Ammonia Synthesis," *ACS Energy Letters* 9 (2024): 3790–3795, https://doi.org/10.1021/acsenergylett.4c01655.

22. D. Shin, Y. Jeon, V. T. Nguyen, et al., "Insight Into Fluoride Additives to Enhance Ammonia Production From Lithium-Mediated Electrochemical Nitrogen Reduction Reaction," *Small* 20 (2024): 2404525, https://doi.org/10.1002/smll.202404525.

23. X. Cai, X. Li, J. You, et al., "Lithium-Mediated Ammonia Electrosynthesis With Ether-Based Electrolytes," *Journal of the American Chemical Society* 145 (2023): 25716–25725, https://doi.org/10.1021/jacs.3c08965.

24. Y. Li, Z. Wang, H. Ji, et al., "Extending Ring-Chain Coupling Empirical Law to Lithium-Mediated Electrochemical Ammonia Synthesis," *Angewandte Chemie International Edition* 63 (2024): e202311413, https://doi.org/10.1002/anie.202311413.

25. C. Lim, D. Kim, M. Kim, et al., "Effect of Sulfur-Derived Solid Electrolyte Interphase on Li-Mediated Nitrogen Reduction," *ACS Energy Letters* 8 (2023): 4875–4884, https://doi.org/10.1021/acsenergylett.3c02038.

26. X. Cai and J. Zhang, "Solvent Effects in Li-mediated Synthesis," *Nature Energy* 9 (2024): 629–630, https://doi.org/10.1038/s41560-024-01538-2.

27. Y. Huan, Y. He, Z. Wang, et al., "Weakened Ionization Electrolyte With n-Hexane Additive Enabling High Activity of Lithium-Mediated Nitrogen Fixation," *Journal of Energy Chemistry* 112 (2026): 39–46, https://doi.org/10.1016/j.jechem.2025.08.037.

28. A. Mangini, J. B. V. Mygind, S. G. Ballesteros, et al., "Multivariate Approaches Boosting Lithium-Mediated Ammonia Electrosynthesis in Different Electrolytes," *Angewandte Chemie International Edition* 137 (2025): e202416027, https://doi.org/10.1002/ange.202416027.

29. H.-L. Du, K. Matuszek, R. Y. Hodgetts, et al., "The Chemistry of Proton Carriers in High-Performance Lithium-Mediated Ammonia Electrosynthesis," *Energy & Environmental Science* 16 (2023): 1082–1090, https://doi.org/10.1039/D2EE03901J.

30. N. Lazouski, K. J. Steinberg, M. L. Gala, D. Krishnamurthy, V. Viswanathan, and K. Manthiram, "Proton Donors Induce a Differential Transport Effect for Selectivity Toward Ammonia in Lithium-Mediated Nitrogen Reduction," *ACS Catalysis* 12 (2022): 5197–5208, https://doi.org/10.1021/acscatal.2c00389.

31. S. Yang, J. Chu, J. Park, H. Kim, and B. Shin, "Enhancement of Lithium-Mediated Nitrogen Reduction by Modifying Center Atom of Tetraalkyl-Type Ionic Liquids," *Angewandte Chemie International Edition* 63 (2024): e202411909, https://doi.org/10.1002/anie.202411909.

32. O. Westhead, R. Tort, J. O. Douglas, et al., "The Role of Ethanol in Lithium-Mediated Nitrogen Reduction," *Journal of the American Chemical Society* 147 (2025): 29687–29701, https://doi.org/10.1021/jacs.5c03389.

33. K. Banerjee, D. T. H. Truong, D. Simondson, et al., "Ammonia-Promoted Lithium Redox-Mediated Nitrogen Reduction," *ACS Energy Letters* 11 (2026): 1958–1964, https://doi.org/10.1021/acsenergylett.5c03719.

34. A. Mangini, A. Garbujo, P. Biasi, et al., "Debunking Pitfalls of Li–N2 Cells for Ammonia Electroproduction: Is This Setup Affordable to Prove Nitro-Fixation before Lithium Plating?," *ACS Electrochemistry* 1 (2025): 2866–2877, https://doi.org/10.1021/acselectrochem.5c00402.

35. F. Duan, J. Chen, M. Zhang, et al., "Lithium-Mediated Ammonia Electrosynthesis Over Orderly Arranged Dipoles Regulated Solid-Electrolyte Interphase," *Journal of the American Chemical Society* 147 (2025): 24317–24325, https://doi.org/10.1021/jacs.5c00551.

36. B. Izelaar, P. Karanth, A. Toghraei, et al., "The Effect of Applied Potential on the Li-Mediated Nitrogen Reduction Reaction Performance," *Nature Communications* 16 (2025): 10635, https://doi.org/10.1038/s41467-025-65627-w.

37. M. S. Iqbal, Y. Ruan, R. Iftikhar, et al., "Lithium-Mediated Electrochemical Dinitrogen Reduction Reaction," *Industrial Chemistry & Materials* 1 (2023): 563–581, https://doi.org/10.1039/D3IM00006K.

38. L. Thapa and C. R. Raj, "Nitrogen Electrocatalysis: Electrolyte Engineering Strategies to Boost Faradaic Efficiency," *Chemsuschem* 16 (2023): e202300465, https://doi.org/10.1002/cssc.202300465.

39. M. Kim, J. Kim, H. Yun, Y. Jeon, Y. J. Hwang, and K. Yong, "Advancing Lithium-Mediated Nitrogen Reduction Using Insights From Lithium-Ion Battery: Focusing on Uniform Li Plating," *Advanced Energy Materials* 16 (2025): e03638, https://doi.org/10.1002/aenm.202503638.

40. Y. Jeon, D. Shin, K. Yong, and Y. J. Hwang, "Enhancing Ammonia Production by Ag Incorporation in Li-Mediated Nitrogen Reduction Reactions," *ACS Energy Letters* 9 (2024): 4147–4152, https://doi.org/10.1021/acsenergylett.4c01438.

41. L.-F. Gao, Y. Cao, C. Wang, et al., "Domino Effect: Gold Electrocatalyzing Lithium Reduction to Accelerate Nitrogen Fixation," *Angewandte Chemie International Edition* 60 (2021): 5257–5261, https://doi.org/10.1002/anie.202015496.

42. Z. T. Wondimkun, T. T. Beyene, M. A. Weret, et al., "Binder-free Ultra-Thin Graphene Oxide as an Artificial Solid Electrolyte Interphase for Anode-Free Rechargeable Lithium Metal Batteries," *Journal of Power Sources* 450 (2020): 227589, https://doi.org/10.1016/j.jpowsour.2019.227589.

43. D. Shin, A. Choi, D.-Y. Han, et al., "Enhancing Lithium-Mediated Nitrogen Reduction With Porous Polymer Fibers Featuring Lithium-Ion Affinity," *Advanced Functional Materials* 35 (2025): 2416484, https://doi.org/10.1002/adfm.202416484.

44. S. Nanda, A. Gupta, and A. Manthiram, "Anode-Free Full Cells: A Pathway to High-Energy Density Lithium-Metal Batteries," *Advanced Energy Materials* 11 (2021): 2000804, https://doi.org/10.1002/aenm.202000804.

45. M. Je, D.-Y. Han, J. Ryu, and S. Park, "Constructing Pure Si Anodes for Advanced Lithium Batteries," *Accounts of Chemical Research* 56 (2023): 2213–2224, https://doi.org/10.1021/acs.accounts.3c00308.

46. Y. Wang, Z. Qu, S. Geng, et al., "Anode-Free Lithium Metal Batteries Based on an Ultrathin and Respirable Interphase Layer," *Angewandte Chemie International Edition* 62 (2023): e202304978, https://doi.org/10.1002/anie.202304978.

47. L. Lin, L. Suo, Y.-S. Hu, H. Li, X. Huang, and L. Chen, "Epitaxial Induced Plating Current-Collector Lasting Lifespan of Anode-Free Lithium Metal Battery," *Advanced Energy Materials* 11 (2021): 2003709, https://doi.org/10.1002/aenm.202003709.

48. Z. Hu, S. Zhang, C. Zhang, and G. Cui, "High Performance Germanium-Based Anode Materials," *Coordination Chemistry Reviews* 326 (2016): 34–85, https://doi.org/10.1016/j.ccr.2016.08.002.

49. Z. Shu and Y. Cai, "Activation of Phosphorene-Like Two-Dimensional GeSe for Efficient Electrocatalytic Nitrogen Reduction via States Filtering of Ru," *Journal of Materials Chemistry A* 9 (2021): 16056–16064, https://doi.org/10.1039/D1TA03420K.

50. X. Wei, C. Chen, X.-Z. Fu, and S. Wang, "Oxygen Vacancies-Rich Metal Oxide for Electrocatalytic Nitrogen Cycle," *Advanced Energy Materials* 14 (2024): 2303027, https://doi.org/10.1002/aenm.202303027.

51. X. Feng, J. Liu, L. Chen, et al., "Hydrogen Radical-Induced Electrocatalytic N_2 Reduction at a Low Potential," *Journal of the American Chemical Society* 145 (2023): 10259–10267, https://doi.org/10.1021/jacs.3c01319.

52. L. M. Azofra, J. M. Doña-Rodríguez, D. R. MacFarlane, and A. N. Simonov, "Mechanism of the N_2 Cleavage Promoted by Lithium vs Other Alkali and Alkaline-Earth Metals," *Journal of Physical Chemistry C* 129 (2025): 1198–1205, https://doi.org/10.1021/acs.jpcc.4c07438.

53. H.-H. Chiang and C.-L. Kuo, "A Comparative First-Principles Study of the Structural and Electronic Properties of the Liquid Li–Si and Li–Ge Alloys," *Journal of Chemical Physics* 146 (2017): 064502, https://doi.org/10.1063/1.4975764.

54. L. Zhang and Z. Cui, "Theoretical Study on Electronic, Magnetic and Optical Properties of Non-Metal Atoms Adsorbed Onto Germanium Carbide," *Nanomaterials* 12 (2022): 1712, https://doi.org/10.3390/nano12101712.

55. W. Chang, A. Jain, F. Rezaie, and K. Manthiram, "Lithium-mediated Nitrogen Reduction to Ammonia via the Catalytic Solid–electrolyte Interphase," *Nature Catalysis* 7 (2024): 231–241, https://doi.org/10.1038/s41929-024-01115-6.

56. S. Li, Y. Zhou, X. Fu, et al., "Long-Term Continuous Ammonia Electrosynthesis," *Nature* 629 (2024): 92–97, https://doi.org/10.1038/s41586-024-07276-5.

57. W. H. Leng, Z. Zhang, J. Q. Zhang, and C. N. Cao, "Investigation of the Kinetics of a TiO_2 Photoelectrocatalytic Reaction Involving Charge Transfer and Recombination Through Surface States by Electrochemical Impedance Spectroscopy," *Journal of Physical Chemistry B* 109 (2005): 15008–15023, https://doi.org/10.1021/jp051821z.

58. A. Tsuneto, A. Kudo, and T. Sakata, "Lithium-Mediated Electrochemical Reduction of High Pressure N_2 to NH_3," *Journal of Electroanalytical Chemistry* 367 (1994): 183–188, https://doi.org/10.1016/0022-0728(93)03025-K.

59. A. Etxebarria, P. Aydogan Gokturk, Y. Ye, P. N. Ross, E. J. Crumlin, and M. Ángel Muñoz-Márquez, "Probing the Surface Chemistry of Lithium Nitridation," *Journal of the American Chemical Society* 147 (2025): 40398–40406, https://doi.org/10.1021/jacs.5c11781.

60. W. Xiao, J. Zhou, L. Yu, D. Wang, and X. W. Lou, "Electrolytic Formation of Crystalline Silicon/Germanium Alloy Nanotubes and Hollow Particles With Enhanced Lithium-Storage Properties," *Angewandte Chemie International Edition* 55 (2016): 7427–7431, https://doi.org/10.1002/anie.201602653.

61. S. Goriparti, U. Gulzar, E. Miele, et al., "Facile Synthesis of Ge–MWCNT Nanocomposite Electrodes for High Capacity Lithium Ion Batteries," *Journal of Materials Chemistry A* 5 (2017): 19721–19728, https://doi.org/10.1039/C7TA04971D.

62. J. Wang, N. Du, H. Zhang, J. Yu, and D. Yang, "Cu–Ge Core–shell Nanowire Arrays as Three-Dimensional Electrodes for High-Rate Capability Lithium-Ion Batteries," *Journal of Materials Chemistry* 22 (2012): 1511–1515, https://doi.org/10.1039/C1JM14430H.

63. E. J. Powell, S. M. Wood, H. Celio, A. Heller, and C. B. Mullins, "Obviating the Need for Nanocrystallites in the Extended Lithiation/De-Lithiation of Germanium," *Journal of Materials Chemistry A* 3 (2015): 23442–23447, https://doi.org/10.1039/C5TA04941E.

64. S. Yoon, C.-M. Park, and H.-J. Sohn, "Electrochemical Characterizations of Germanium and Carbon-Coated Germanium Composite Anode for Lithium-Ion Batteries," *Electrochemical and Solid-State Letters* 11 (2008): A42, https://doi.org/10.1149/1.2836481.

65. H. Jung, P. K. Allan, Y.-Y. Hu, et al., "Elucidation of the Local and Long-Range Structural Changes That Occur in Germanium Anodes in Lithium-Ion Batteries," *Chemistry of Materials* 27 (2015): 1031–1041, https://doi.org/10.1021/cm504312x.

66. C. Zhong, J.-Z. Wang, X.-W. Gao, D. Wexler, and H.-K. Liu, "In Situ One-Step Synthesis of a 3D Nanostructured Germanium–Graphene Composite and Its Application in Lithium-Ion Batteries," *Journal of Materials Chemistry A* 1 (2013): 10798, https://doi.org/10.1039/c3ta11796k.

67. Z. Chen, Y. Yan, S. Xin, et al., "Copper Germanate Nanowire/Reduced Graphene Oxide Anode Materials for High Energy Lithium-Ion Batteries," *Journal of Materials Chemistry A* 1 (2013): 11404, https://doi.org/10.1039/c3ta12344h.

68. L. Y. Lim, N. Liu, Y. Cui, and M. F. Toney, "Understanding Phase Transformation in Crystalline Ge Anodes for Li-Ion Batteries," *Chemistry of Materials* 26 (2014): 3739–3746, https://doi.org/10.1021/cm501233k.

69. L. Baggetto, E. J. M. Hensen, and P. H. L. Notten, "In Situ X-Ray Absorption Spectroscopy of Germanium Evaporated Thin Film Electrodes," *Electrochimica Acta* 55 (2010): 7074–7079, https://doi.org/10.1016/j.electacta.2010.06.087.

70. A. Karen, K. Ito, and Y. Kubo, "TOF-SIMS Analysis of Lithium Air Battery Discharge Products Utilizing Gas Cluster Ion Beam Sputtering for Surface Stabilization," *Surface and Interface Analysis* 46 (2014): 344–347, https://doi.org/10.1002/sia.5508.

71. Y. Zhao, S.-K. Otto, T. Lombardo, et al., "Identification of Lithium Compounds on Surfaces of Lithium Metal Anode With Machine-Learning-Assisted Analysis of ToF-SIMS Spectra," *ACS Applied Materials & Interfaces* 15 (2023): 50469–50478, https://doi.org/10.1021/acsami.3c09643.

72. S. Wenzel, S. Randau, T. Leichtweiß, et al., "Direct Observation of the Interfacial Instability of the Fast Ionic Conductor $Li_{10}GeP_2S_{12}$ at the Lithium Metal Anode," *Chemistry of Materials* 28 (2016): 2400–2407, https://doi.org/10.1021/acs.chemmater.6b00610.

73. W. Li, P. Shen, L. Yang, et al., "Novel Cu(Zn)–Ge–P Compounds as Advanced Anode Materials for Li-ion Batteries," *Energy & Environmental Science* 14 (2021): 2394–2407, https://doi.org/10.1039/D0EE03553J.

74. T. Yoon, G. Song, A. M. Harzandi, et al., "Intramolecular Deformation of Zeotype-Borogermanate Toward a Three-Dimensional Porous Germanium Anode for High-Rate Lithium Storage," *Journal of Materials Chemistry A* 6 (2018): 15961–15967, https://doi.org/10.1039/C8TA04626C.

75. W. Tao, H. Chun, S. Hyun, and B. Han, "Design a Multiphase Interfaced Ge(GeO)/T-Nb_2O_5−/C Anode With Synergistic High Capacity and Durability for Li-ion Batteries," *Applied Surface Science* 640 (2023): 158424, https://doi.org/10.1016/j.apsusc.2023.158424.

76. K. Li, S. Z. Andersen, M. J. Statt, et al., "Enhancement of Lithium-Mediated Ammonia Synthesis by Addition of Oxygen," *Science* 374 (2021): 1593–1597, https://doi.org/10.1126/science.abl4300.

77. C. Lim, Y. Sohn, M. Kwon, D.-H. Seo, W. Kim, and K. Yong, "Suppressing Anion Repulsion for Enhancing Li-Mediated Nitrogen Reduction," *ACS Energy Letters* 10 (2025): 5796–5808, https://doi.org/10.1021/acsenergylett.5c02721.

78. Y. Han, C. Lim, Y. Kim, et al., "Steric Hindrance-Derived Li^+ Solvation to Enhance Lithium-Mediated Nitrogen Reduction," *ACS Energy Letters* 9 (2024): 5509–5519, https://doi.org/10.1021/acsenergylett.4c02626.

79. N. Lazouski, M. Chung, K. Williams, M. L. Gala, and K. Manthiram, "Non-Aqueous Gas Diffusion Electrodes for Rapid Ammonia Synthesis From Nitrogen and Water-Splitting-Derived Hydrogen," *Nature Catalysis* 3 (2020): 463–469, https://doi.org/10.1038/s41929-020-0455-8.

80. X. Fu, J. B. Pedersen, Y. Zhou, et al., "Continuous-Flow Electrosynthesis of Ammonia by Nitrogen Reduction and Hydrogen Oxidation," *Science* 379 (2023): 707–712, https://doi.org/10.1126/science.adf4403.

81. B. H. R. Suryanto, K. Matuszek, J. Choi, et al., "Nitrogen Reduction to Ammonia at High Efficiency and Rates Based on a Phosphonium Proton Shuttle," *Science* 372 (2021): 1187–1191, https://doi.org/10.1126/science.abg2371.

82. S. Z. Andersen, M. J. Statt, V. J. Bukas, et al., "Increasing Stability, Efficiency, and Fundamental Understanding of Lithium-Mediated Electrochemical Nitrogen Reduction," *Energy & Environmental Science* 13 (2020): 4291–4300, http://doi.org/10.1039/D0EE02246B.

Supporting Information

Additional supporting information can be found online in the Supporting Information section.

Supporting File: anie72873-sup-0001-SuppMat.docx.